Effect of supports on the kind of in-situ formed ZnO_x species and its consequence for non-oxidative propane dehydrogenation

Dan Zhao[a, §], Vita A. Kondratenko[a], Dmitry E. Doronkin[b], Shanlei Han[a], Jan-Dierk Grunwaldt[b], Uwe Rodemerck[a], David Linke[a], Evgenii V. Kondratenko[a*]

[a] Leibniz-Institut für Katalyse e. V., 18059 Rostock, Germany

[b]Institute of Catalysis Research and Technology and Institute for Chemical Technology and Polymer Chemistry, Karlsruhe Institute of Technology (KIT), 76131 Karlsruhe, Germany

[§]Current address: Institute of Catalysis Research and Technology, Karlsruhe Institute of Technology (KIT), 76344 Eggenstein-Leopoldshafen, Germany

*Correspondence to evgenii.kondratenko@catalysis.de

Abstract

Non-oxidative propane dehydrogenation (PDH) to propene is the basis of various large-scale processes suffering however from high costs and environmental incompatibility of currently applied Pt- or Cr-containing catalysts. Herein, we demonstrate that active and selective catalysts can be obtained from cheap and commercially available Zr- or Ti-based supports and ZnO without producing any liquid or solid waste. Catalytically active species formed in situ under PDH conditions are composed of isolated ZnO_x as concluded from X-ray absorption spectroscopic analysis. The kind of support affects the geometry of such species that is probably decisive for catalyst activity. ZnO_x on the surface of $LaZrO_x$ revealed the highest Zn-related TOF of propene formation. However, the following activity order in terms of space time yield of propene formation (STY_{C3H6}) at 550°C and about 50% equilibrium propane conversion using a feed with 40vol% propane was obtained: $ZnO//TiZrO_x$ > $ZnO//SiZrO_x$ > $ZnO//LaZrO_x$ > $ZnO//TiO_2$. The best-performing catalyst showed STY_{C3H6} of 2 kg kg_{cat}^{-1} h^{-1} and was durable in 8 PDH/regeneration cycles. Temporal analysis of products with submillisecond resolution suggests that H_2 formation should be the rate-determining step in the course of the PDH reaction.

Keywords: ZnO_x-containing catalysts; commercially available materials; propane dehydrogenation; reaction mechanisms

Highlights:

- Catalysts consisting of ZnO and commercially available supports were tested in PDH
- The developed ZnO//$TiZrO_x$ catalyst showed high activity, selectivity and durability
- The formation of H_2 was concluded to be the rate-determining step

1 Introduction

Propene production through non-oxidative dehydrogenation of propane (PDH) is attracting more and more attention both from academic and industrial fields due to the high carbon efficiency and the availability of propane[1-3]. Currently, the commercial PDH processes are using Pt-based or Cr-based catalysts. Although they are highly active and selective, they suffer from some shortcomings related to high costs of platinum or toxicity of Cr(VI) compounds. Against this background, many catalysts based on non-noble metal oxides, such as VO_x[4-6], GaO_x[7], CoO_x[8, 9], FeO_x[10], SnO_x[11], InO_x[12], ZrO_2[13, 14], TiO_2[15, 16] and Al_2O_3[17, 18], have been developed and tested in the PDH reaction. ZnO_x-based catalysts are also promising for the PDH reaction due to their environmental compatibility and their ability to active C–H bond selectively[19-27].

Very recently[27, 28], we have developed a simple method to prepare ZnO_x-containing catalysts using commercial ZnO and siliceous zeolites. The catalyst preparation method is ecologically friendly as neither solid nor liquid waste is produced. The solid catalyst components are simply physically mixed. Catalytically active ZnO_x sites are formed on the zeolite surface directly under PDH conditions. The first step behind their formation is the reduction of ZnO by H_2 or C_3H_8 to metallic Zn ($ZnO + H_2 \rightarrow Zn + H_2O$) at temperatures above the melting point of this metal (~ 420 °C). In the second step, the generated gas-phase Zn atoms react with zeolite OH nests as follows: $2Zn + 2x–OH \rightarrow 2ZnO_x + xH_2\uparrow$. The optimized ZnO-Silicalite-1 catalyst showed about 3 times higher propene productivity and comparable propene selectivity in comparison with a commercial-like K-CrO_x/Al_2O_3 catalyst at similar degrees of propane conversion under industrially relevant conditions. Although the developed catalyst outperformed many state-of-the-art ZnO-based catalysts in terms of space time yield of propene formation, expensive siliceous zeolites have to be used as supports. Such materials can only be synthesized in the presence of structure-directing agents (SDAs), e.g., quaternary ammonium

bases/salts, or through a dealumination process using a concentrated inorganic acid, such as HNO_3. The expensive SDAs have to be removed to obtain high a2qyay surface area through calcining zeolite precursors that is, however, environmentally unfriendly. The dealumination process also produces a lot of liquid waste and the prepared materials are not thermally stable at high temperatures due to many framework defects[29].

Motivated by the above-mentioned shortcomings of zeolites, the current study is aimed to check (i) if commonly used metal oxides can be applied as supports to capture metallic Zn atoms, forming catalytically active ZnO_x species and to elucidate (ii) the effects of these supports on catalyst performance, the kind of active sites and the rate-determining step in the PDH reaction. To this end, commercially available TiO_2, $TiZrO_x$, $SiZrO_x$ or $LaZrO_x$ supports and bare ZnO were used for catalyst preparation without producing any liquid or solid waste. By means of X-ray absorption spectroscopy (XAS), the specific ZnO_x structures were determined to be single ZnO_x sites over all prepared catalysts but with different geometries. The temporal analysis of products (TAP) results revealed that H_2 formation is the rate-determining step in the PDH reaction, and it is strongly affected by the kind of support.

2 Experimental section

2.1 Materials and catalyst preparation

Commercial ZnO (Sigma-Aldrich), TiO_2 (rutile TiO_2, Sachtleben Chemie GmbH), $LaZrO_x$ (9wt% La_2O_3, Daiichi Kigenso Kagaku Kogyo Co), $TiZrO_x$ (30% TiO_2, Daiichi Kigenso Kagaku Kogyo Co) and $SiZrO_x$ (96 wt% ZrO_2) were used without any further treatment. For catalytic tests (see section 2.2.4 and 2.2.5), the materials were pressed and crushed to get particles of 315-710 μm. ZnO and each support were loaded into a quartz tubular reactor in the form of two layers as shown in Scheme 1a. These two layers were separated by a layer of quartz

wool (about 5 mg) to avoid any physical contact. The materials used for catalytic performance were named as ZnO//support.

To exclude the effect of bulk ZnO on X-ray absorption spectroscopic measurements (see section 2.2.2) and transient studies (see section 2.2.3), we prepared additional materials as follows. ZnO (20 mg, 315-710 μm) and a selected support material (50 mg, 315-710 μm) were loaded into a quartz reactor with ZnO being the top layer (Scheme 1a). The samples were initially heated to 550 °C in a flow of N_2 (10 mL·min^{-1}) then flushed with air (10 mL·min^{-1}) at the same temperature for 1 h. After 15 min purging in N_2, a flow of 50 vol% H_2 in N_2 (10 mL min^{-1}) was fed at 550 °C for 2 h. Then, the bottom layer was collected for catalyst characterization (Scheme 1b). The materials prepared according to this method were named as ZnO-support to distinguish them from the catalysts used for the catalytic tests. The Zn loading in ZnO-TiO_2, ZnO-$LaZrO_x$, ZnO-$SiZrO_x$ and ZnO-$TiZrO_x$ is 2.13, 0.92, 3.11 and 2.40 wt%, respectively.

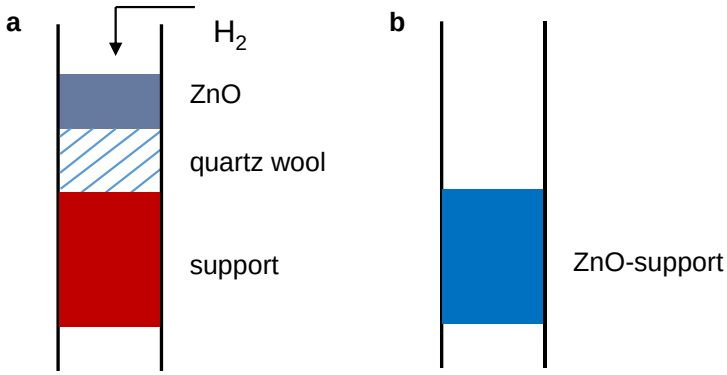

Scheme 1 A schematic illustration of reactor loading for the dual-bed reduction method (a), the collected catalyst used for XAS measurements and transient studies(b).

2.2 Catalyst characterization

2.2.1 N_2 adsorption–desorption tests

To determine the specific surface area (S_{BET}) of fresh, as-prepared and spent (after about 60 h durability test) samples, N_2 adsorption-desorption measurements were carried out using the

ASAP 2020 (Micromeritics, USA) instrument. The samples were initially heated to 300 °C in N_2 for 4 h to remove physically adsorbed water. After that, N_2 adsorption–desorption measurements were carried out at 77 K.

2.2.2 X-ray absorption spectroscopy

X-ray absorption spectroscopy (XAS) was applied to reveal the local structures of materials prepared according to Scheme 1. X-ray absorption near energy structure (XANES) and extended X-ray absorption fine structure (EXAFS) spectra at the Zn K absorption edge were recorded at the P65 beamline of the PETRA III synchrotron (DESY, Hamburg) in fluorescence mode. The energy of the X-ray photons was selected by a Si(111) double-crystal monochromator and the beam size was set to 0.2(vertical) × 1.5(horizontal) mm^2. The spectra were normalized, and the EXAFS background was subtracted using the ATHENA program from the Demeter software package[30]. The k^2-weighted EXAFS functions were Fourier transformed (FT) in the k range of 2-10 $Å^{-1}$. Then the amplitude reduction factor S_0^2=1.06 was obtained by fitting the ZnO reference spectrum to a wurtzite structural model as reported in the Crystallography Open Database (ZnO, COD ID. 1011259). The fits of the EXAFS data were performed using Artemis by a least square method in R-space between 1.0 and 3.0 Å. Coordination numbers (CN), interatomic distances (r), energy shift (δE_0) and mean square deviation of interatomic distances (σ^2) were refined during fitting. The absolute misfit between theory and experiment was expressed by ρ.

2.2.3 Temporal analysis of products

Individual pathways of product formation in the PDH reaction was analyzed using a temporal analysis of products (TAP-2) reactor, a pulse technique operating with a time resolution of around 100 μs described in details in Refs. [31, 32]. ZnO-$TiZrO_x$ (48 mg) and ZnO-$LaZrO_x$ (62 mg) used in this study were prepared by the dual-bed method (Scheme 1a). Each catalyst (sieve fraction of 315–710 μm) was packed between two layers of quartz particles

(sieve fraction of 250–350 μm) within the isothermal zone of micro-reactor made of quartz. Before the tests the catalysts were heating in an Ar flow from room temperature to 550°C and then exposed to a flow of 20 vol% O_2 in Ar (10 mL min^{-1}) for 0.5 h at the same temperature. Subsequently the catalysts were reduced in a flow of 50 vol% H_2 in Ar for 0.5 h at 550°C. Hereafter, the micro-reactor was exposed to vacuum of about 10^{-5} Pa and pulse experiments were performed at 550 °C using a C_3H_8/Ar=1:1 mixture. The mixture was prepared using C_3H_8 (Linde, 3.5) and Ar (Air Liquide, 5.0) without additional purification. The total pulse size was kept between 6-7·× 10^{15} molecules per pulse.

The feed components and the reaction products were monitored using an on-line quadrupole mass spectrometer (HAL RD 301 Hiden Analytical) at m/z (AMU) of 44 (C_3H_8), 42 (C_3H_8, C_3H_6), 41 (C_3H_8, C_3H_6), 30 (C_2H_6), 29 (C_3H_8, C_2H_6), 28 (C_3H_8, C_2H_6, C_2H_4), 27 (C_3H_8, C_2H_6, C_2H_4), 26 (C_3H_8, C_2H_6, C_2H_4), 18 (H_2O), 16 (CH_4), 2 (H_2) and 40 (Ar). For each m/z, the pulses were repeated ten times and averaged to improve the signal-to-noise ratio. The concentration of the feed components and the reaction products was determined from the respective m/z using standard fragmentation patterns and sensitivity factors determined in separate calibration tests.

The normalization of the recorded responses was carried out for an easier comparison of the position of the maximal concentration (t_{max}) of the feed components and reaction products. In order to take into account the different diffusion velocities of these compounds the experimental time was transformed to a dimensionless time using equation 1 as specified in Ref. [33].

$$Dimensionless\ time = \frac{t \times D^{eff}_{Knudsen}(i)}{L^2} \qquad \text{eq. 1}$$

Where t is the experimental time, $D^{eff}_{Knudsen}(i)$ is the diffusion coefficient of C_3H_8, C_3H_6, CH_4, H_2 or Ar and L is the diffusion length. The diffusion coefficients of C_3H_8, C_3H_6, CH_4 and H_2

were calculated from that of Ar according to eq. 2. The diffusion coefficient of Ar was determined through fitting the experimental response of this gas to the Knudsen diffusion model, as described in Ref. [34].

$$D_{Knudsen}^{eff}(i) = D_{Knudsen}^{eff}(Ar) \times \sqrt{\frac{M(Ar)}{M(i)}} \qquad \text{eq. 2}$$

The diffusion length for C_3H_8 corresponded to the reactor length, while for the reaction products C_3H_6, CH_4 and H_2 it was equal to the distance from the beginning of the catalyst layer to the reactor outlet.

2.2.4 Initial activity tests

Propane dehydrogenation tests were performed using an in-house built setup equipped with 15 continuous-flow fixed-bed tubular reactors made of quartz. To determine the rate of propene formation, the degree of propane conversion was controlled below 15% of the equilibrium propane conversion under the same reaction conditions. Typically, 50 mg of support and 20 mg of ZnO were loaded into reactors as shown in Scheme 1a. A reaction feed (40 mL·min^{-1} in total) consisting of 40 vol% C_3H_8 in N_2 was used for the tests. The catalysts were initially heated to 550 °C in a flow of N_2 (10 mL·min^{-1}) and then flushed with a flow of air (10 mL·min^{-1}) at the same temperature for 1 h. After 15 min N_2 purging, a flow of 50 vol% H_2 in N_2 (10 mL·min^{-1}) was fed at the same temperature to generate supported ZnO_x species. The duration of the reductive treatment was 1 h or 2 h. The rate of propene formation was calculated according to eq. 3. Propene selectivity was higher than 99% and carbon balance values were close to 100%. The Zn-related turnover frequency (TOF) was calculated using equation 4.

$$r(C_3H_6) = \frac{\dot{n}_{C_3H_6}^{out}}{m_{cat}} \qquad \text{eq.3}$$

$$TOF = \frac{r_{C_3H_6}}{n_{Zn}} \qquad \text{eq. 4}$$

where $\dot{n}_{C_3H_8}^{out}$ and m_{cat} mean the molar flow rate (mmol·min^{-1}) of C_3H_6 at the outlet of reactor and the mass (g) of catalyst. It should be specially mentioned that only the mass of support was considered for such calculation. n_{Zn} is the molar weight of Zn in the prepared catalyst.

2.2.5 Durability tests

Durability tests were performed at 550 °C. The pretreatment steps were same as applied for the initial activity tests. The reduction time was 2 h at the same temperature. After each PDH cycle lasting for 28 min, the spent catalysts were oxidized in a flow of air (10 mL min^{-1}) for 30 min. After 15 min N_2 purging (10 mL min^{-1}), they were further reduced in H_2 at the same temperature for 30 min. Before the next PDH test, the reduced catalysts were purged again in a flow of N_2 (10 mL min^{-1}) for 15 min. The conversion of propane ($X(C_3H_8)$), the selectivity to propene ($S(C_3H_6)$), cracking products (S(cracking products)) and coke (S(coke)) as well as the space-time yield of propene formation ($STY(C_3H_6)$) were calculated according to eqs. 5-9, respectively. Equation 10 was used to calculate an apparent constant of catalyst deactivation rate.

$$X(C_3H_8)=\frac{\dot{n}_{C_3H_8}^{in}-\dot{n}_{C_3H_8}^{out}}{\dot{n}_{C_3H_8}^{in}} \quad \text{eq. 5}$$

$$S(i)=\frac{\beta_i}{\beta_{C_3H_8}}\frac{\dot{n}_i^{out}}{\dot{n}_{C_3H_8}^{in}-\dot{n}_{C_3H_8}^{out}} \quad \text{eq. 6}$$

$$S(\text{cracking products})=S(CH_4)+S(C_2H_4) \quad \text{eq.7}$$

$$S(\text{coke})=1-\sum_i S(i) \quad \text{eq. 8}$$

$$STY=\frac{\dot{n}_{C_3H_6}\times M_{C_3H_6}\times 60}{1000\times m_{cat}} \quad \text{eq. 9}$$

$$k_{deactivation}=\frac{\ln\left(\frac{1-X(C_3H_8)_{final}}{X(C_3H_8)_{final}}\right)-\ln\left(\frac{1-X(C_3H_8)_{initial}}{X(C_3H_8)_{initial}}\right)}{t} \quad \text{eq. 10}$$

where "$\dot{n}_{in}$" and "$\dot{n}_{out}$" stand for the molar flows of gas-phase components at the reactor inlet and outlet, respectively. N_2 was used as an internal inert standard to consider the reaction-induced changes in the number of moles. $X(C_3H_8)_{initial}$ and $X(C_3H_8)_{final}$ stand for the propane conversion after 4 min and after 28 min on propane stream, respectively. t is 0.467 h.

The gas-phase products and the feed components were analyzed by an on-line gas chromatograph (Agilent 6890) equipped with flame ionization and thermal conductivity detectors. The time taken for product analysis was 4 min. The gas chromatograph was equipped with PLOT/Q (for CO_2), AL/S (for hydrocarbons), and Molsieve 5 (for H_2, O_2, N_2, and CO) columns.

3 Results and discussion

3.1 Catalytic performance

As mentioned in the experimental part, catalytic tests were carried out using catalysts simply consisting of separated ZnO and support layers located in the reactor as shown in Figure 1a. The rate of propene formation ($r(C_3H_6)$) at 550°C over these catalysts after different reduction times and over the corresponding bare supports is present in Figure 1b. A commercial-like K-CrO_x/Al_2O_3 catalyst was used for benchmarking of the developed catalysts. The dashed line in Figure 1b stands for the rate obtained over this catalyst. In comparison with this reference material, the ZnO//$LaZrO_x$, ZnO//$SiZrO_x$ and ZnO//$TiZrO_x$ catalysts showed comparable or superior activity. The ZnO//TiO_2 catalyst was less active.

It is also clearly seen in Figure 1b that the bare supports showed significantly lower activity than the Zn-containing catalysts under the same reaction conditions. Depending on the kind of support, the propene formation rate is in the range of 0.05 to 0.3 mmol g^{-1} min^{-1}. The activity was improved by 2.9-17.2 times when ZnO layer was present on the top of support layer (Figure S1). The strength of the enhancement depends on the kind of support and the duration of

reductive catalyst treatment (Figure S1). For example, when the catalysts were reduced for 1 h, the ratio of $r(C_3H_6)_{\text{with ZnOx}}$ to $r(C_3H_6)_{\text{bare support}}$ is 16.9, 3.5, 13.9 and 9.1 for TiO_2, $LaZrO_x$, $SiZrO_x$ and $TiZrO_x$ support, respectively. When the reduction time was increased to 2 h, such values increased further for the ZnO//$SiZrO_x$ and ZnO//$TiZrO_x$ catalysts but decreased slightly for the ZnO//TiO_2 and ZnO//$LaZrO_x$ materials.

In the light of different loadings of Zn in the catalysts, for a proper comparison of their activity, we calculated Zn-related TOF values under consideration that each ZnO_x species is active in the PDH reaction (eq. 4). The calculated TOF value is424, 185, 164 and 126 h^{-1} for ZnO//$LaZrO_x$, ZnO//TiO_2, ZnO//$TiZrO_x$ and ZnO//$SiZrO_x$ samples (Figure 1c), respectively. The ZnO species on the surface of $LaZrO_x$ seems to be the most active catalyst.

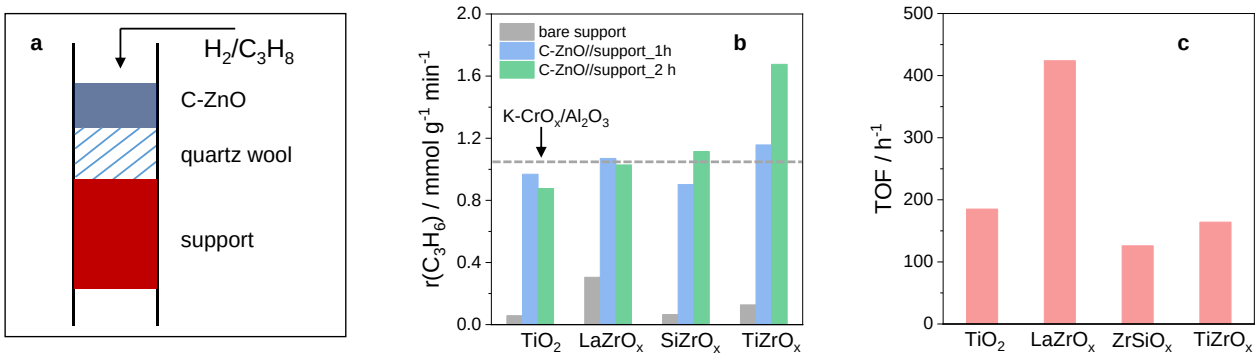

Figure 1 (a) A schematic illustration of reactor loading for catalytic tests; (b) the rate of propene formation ($r(C_3H_6)$) over bare supports and ZnO//support samples with different reduction time. Reaction conditions: 550 °C, 50 mg of support, 20 mg of commercial ZnO, C_3H_8:N_2=4:6, 40 mL·min^{-1} of total flow. The dashed line means the $r(C_3H_6)$ value of the commercial-like K-CrO_x/Al_2O_3 catalyst. (c) The Zn-related TOF values of propene formation over different catalysts (eq. 4).

3.2 The nature of active sites

As reported in previous studies[13-18], coordinatively unsaturated Zr^{4+} (Zr_{cus}^{4+}), Ti^{4+} (Ti_{cus}^{4+}) or Al^{3+} (Al_{cus}^{3+}) sites generated upon a reductive treatment of catalysts based on ZrO_2, TiO_2 or Al_2O_3 are the active sites in the PDH reaction. To check if this statement is also valid for the

ZnO//support catalysts tested in the present study, we determined apparent activation energies of propane conversion over the bare supports and the catalysts in the temperature range of 500-550 °C. The obtained E_a values are summarized in Table 1 and the corresponding Arrhenius plots are presented in Figure S2. Bare ZrO_2-based materials have the highest E_a values ranging between 170 and 225 kJ·mol^{-1}, which are in line with our previous studies[13, 14]. Bare TiO_2 has the lowest E_a value among the support materials of 120 kJ·mol^{-1}. The E_a values of ZnO//support are 31-76 kJ·mol^{-1} lower than those of the bare supports. For instance, E_a decreased from 172 kJ·mol^{-1} to 96 kJ mol^{-1} when Zn was introduced to the $TiZrO_x$ support. The change in the E_a values suggests that the active sites in the ZnO_x-containing samples are different from those in the bare supports. Therefore, we put forward that supported ZnO_x species should be the active sites rather than coordinatively unsaturated Zr^{4+} or Ti^{4+} cations.

Table 1 Apparent activation energies of propane conversion over different catalysts tested in the PDH reaction in the temperature range of 500-550 °C.

Support	E_a / kJ mol^{-1}	ZnO//Support	E_a / kJ mol^{-1}
TiO_2	120	ZnO//TiO_2	89
$LaZrO_x$	225	ZnO//$LaZrO_x$	155
$SiZrO_x$	182	ZnO//$SiZrO_x$	117
$TiZrO_x$	172	ZnO//$TiZrO_x$	96

To gain an insight into the structure of supported ZnO_x species at an atomic level, we applied X-ray absorption spectroscopy (XAS). To avoid the effect of bulk ZnO on the measurements, the characterized materials were prepared according to Scheme 1. Metallic Zn and ZnO were used as the references to represent the absorption edges of Zn^0 and Zn^{2+}, respectively. As seen in Figure 2a, the position of the absorption edges of all ZnO_x species is the same as that of the ZnO. This indicates that the oxidation state of Zn in the prepared catalysts is +2. The Fourier

transformed k^2-weighed EXAFS spectra are present in Figure 2b. The fitting results are summarized in Table 2 while the fits are given in Figure S3. For all catalysts, the first Zn-O shell scattering is visible at about 1.5 Å (uncorrected distance) but with different coordination numbers (CNs) based on EXAFS fits. The average CNs of Zn-O in ZnO-$LaZrO_x$ and ZnO-TiO_2 are 2.9 and 4.0, respectively. The corresponding values for ZnO-$TiZrO_x$ and ZnO-$SiZrO_x$ are slightly lower, i.e., 2.6 and 2.7, respectively. For the second shell scattering at about 3 Å, we firstly considered a Zn-Zn path. However, negative values and relatively high Debye-Waller factors of about 0.03 were obtained from the fits. Thus, any Zn-Zn path was not considered for the catalysts. When $LaZrO_x$ and TiO_2 supports were used, Zn-La and Zn-Ti paths fitted well at about 3 Å although relatively low CNs of 0.9 and 0.6 were obtained, respectively. It may suggest a strong interaction between ZnO_x species and the supports. In the case of ZnO-$TiZrO_x$ and ZnO-$SiZrO_x$, neither Zn-Zn, Zn-Zr, Zn-Ti nor Zn-Si paths could be fitted well. However, the quality of the fit was strongly improved in the presence of Zn-O path at a longer distance (about 3.2 Å). Thus, the CN of Zn-O in these two materials is about 4 in total. In summary, as no reasonable CN of Zn-Zn could be derived from the fits, all tested materials should possess isolated ZnO_x species but with different geometries.

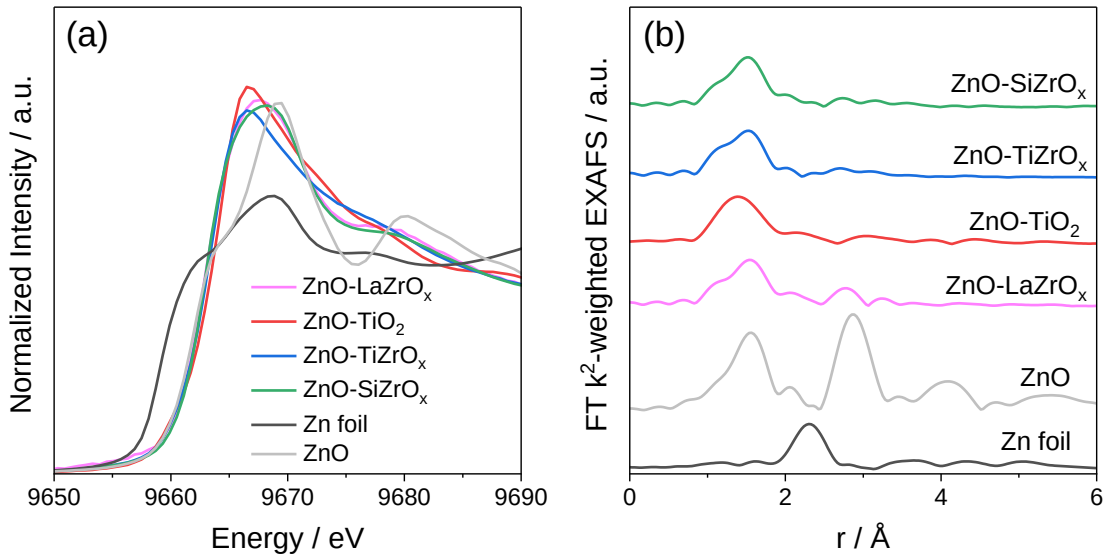

Figure 2 (a) The XANES spectra of different ZnO-support catalysts at the Zn K edge. (b) The corresponding Fourier transformed k^2-weighted EXAFS spectra.

Table 2 EXAFS fitting results

catalyst	shell	CN	distance (Å)	δ^2 (10^{-3} Å^2)	ΔE_0	ρ
ZnO-$LaZrO_x$	Zn-O	2.9 ± 0.5	2.04 ± 0.02	9 ± 3	3.22 ± 1.2	0.052
	Zn-La	0.9 ± 0.4	2.97 ± 0.03	5 ± 6		
ZnO-TiO_2	Zn-O	4.0 ± 0.2	1.96 ± 0.007	10 ± 1	2.57 ± 0.55	0.005
	Zn-Ti	0.6 ± 0.2	2.93 ± 0.03	10 ± 1		
ZnO-$TiZrO_x$	Zn-O	2.6 ± 0.3	2.00 ± 0.01	6 ± 2	1.2 ± 0.95	0.027
	Zn-O	1.3 ± 0.5	3.19 ± 0.04	6 ± 2		
ZnO-$SiZrO_x$	Zn-O	2.7 ± 0.3	2.01 ± 0.01	6 ± 2	2.07 ± 1.06	0.029
	Zn-O	0.8 ± 0.6	3.22 ± 0.08	6 ± 2		

3.3 Rate-limiting step in the PDH reaction

To determine kinetically relevant steps in the PDH reaction, pulse experiments with C_3H_8 were performed in the temporal analysis of products (TAP-2) reactor. Similar to the XAS studies (section 3.2) the catalysts used in these tests were prepared by the dual-bed method (Scheme 1) in order to exclude the effect of bulk ZnO. Two catalysts (ZnO-$TiZrO_x$ and ZnO-$LaZrO_x$) were selected based on their steady-state catalyst performance. ZnO-$TiZrO_x$ was the most active and selective and its activity increased with catalyst reduction time (Figure 1). ZnO-$LaZrO_x$ was less selective, and its activity slightly decreased with the reduction time. Before the transient tests, the catalysts were treated in the similar way as in previously described PDH tests. C_3H_6, H_2 and CH_4 was observed upon C_3H_8 pulsing. The height-normalized responses of C_3H_8 and these gas-phase products are shown in Figure 3. As suggested in Ref. [33], the X-axis has been transformed into a dimensionless form (eq.1) to exclude the effect of difference diffusivity rates on the appearance order of the reaction products and the feed components.

As it can be expected for the feed component, which reacts, the response of C_3H_8 is the narrowest one and has the lowest time (t_{max}) of its maximal value (Figure 3). The shape of the

C_3H_6, H_2 and CH_4 responses is broader. They are also characterized by higher t_{max} values, which can be ordered as follows $t_{max}(C_3H_6) < t_{max}(CH_4) \ll t_{max}(H_2)$. The t_{max} value of C_3H_6 is quite similar for both catalysts. However, the position and the shape of CH_4 and H_2 responses depend on the catalyst. They are broader over ZnO-$LaZrO_x$ and the maximum of the H_2 response is shifted to longer time. These differences are explained by the lower activity of this catalyst towards formation of these products. As the CH_4 response appears after the C_3H_6 response, we can conclude that C_3H_6 undergoes further cracking reactions yielding CH_4. This is in agreement with our previous study of the PDH reaction over various ZnO-based catalysts[35, 36]. Importantly, the t_{max} of H_2 is significantly greater than that of C_3H_6. This means that the formation of hydrogen is much slower in comparison with the formation of propene. In other words, the cleavage of C-H bonds in C_3H_8 is faster than the recombination of surface hydrogen species and the latter process is the rate-limiting step in the course of PDH reaction. In addition,

the t_{max} of H_2 over ZnO-$TiZrO_x$ is lower than that over ZnO-$LaZrO_x$ (Figure 3). Thus, the presence of Ti seems to facilitate the recombination of H atoms on the surface of the catalyst.

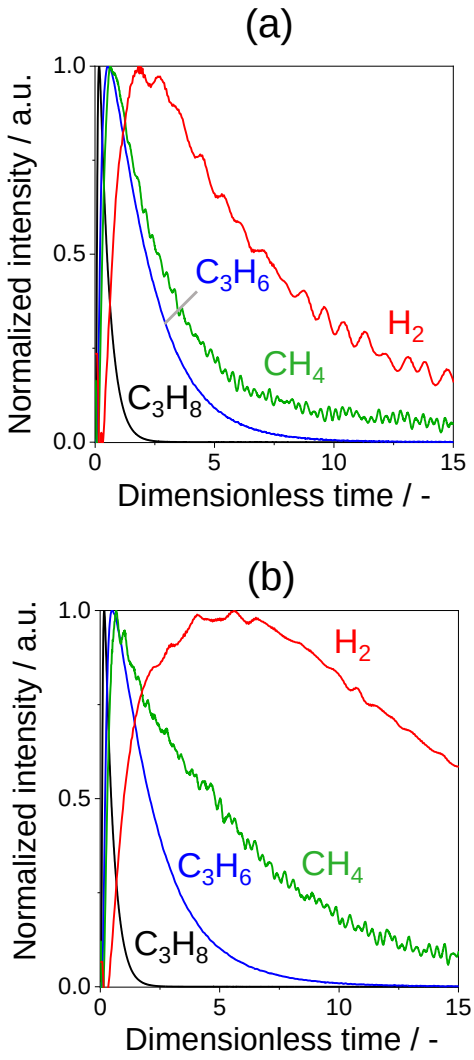

Figure 3 Height-normalized transient responses of C_3H_8, C_3H_6, CH_4 and H_2 after pulsing of a C_3H_8 : Ar=1 : 1 mixture over (a) ZnO-$TiZrO_x$ and (b) ZnO-$LaZrO_x$ catalysts at 550°C.

3.4 Application potential of developed catalysts and benchmarking

The developed catalysts were also tested under industrially relevant conditions at 550 °C in a series of 8 PDH/regeneration cycles to check their durability. Prior to the PDH reaction, a reduction treatment was required to generate active ZnO_x species over the supports. Propane conversion, propene selectivity and selectivity to coke and cracking products are shown in Figures S4 and S5. The initial propane conversion (after 4 min) over all catalysts is in the range

of 0.2-0.24 which was controlled through varying the contact time for different catalysts. This conversion level is about 50% of the equilibrium conversion. For all catalysts, the conversion decreased within 28 min on propane stream (Figure S4). The deactivation rate constant calculated according to eq. 10 can be ordered as follows: ZnO//$LaZrO_x$ > ZnO//$TiZrO_x$ > ZnO//$SiZrO_x$ > ZnO//TiO_2 (Table 3). For the durability test, we distinguished two different kinds of catalyst deactivation. As seen in Figure S4, propane conversion (i) decreased within a PDH test (28 min) or (ii) cannot be fully recovered from cycle to cycle. According to our previous studies[25, 27], there are two possible reasons responsible for the first kind of catalyst deactivation, i.e., (i) coke formation and (ii) loss of Zn from the catalysts. As we had an available ZnO upper layer to supply Zn atoms continuously during the PDH test, the latter reason of catalyst deactivation within one PDH cycle could be excluded. This statement is also supported by the fact that the conversion over the ZnO//$LaZrO_x$, ZnO//$TiZrO_x$ and ZnO//$SiZrO_x$ catalysts can be fully recovered to the initial value after an oxidative catalyst regeneration (Figures S4 and S5). Thus, coke formation should be the main reason for the deactivation within one PDH cycle. For the ZnO//TiO_2 catalyst, the initial propane conversion (first data point in each cycle), however, decreased from 22.3% to 18.9% from 1st cycle to 8th cycle (Figure S4). This is an indication that there is at least an additional reason causing catalyst deactivation. As seen in Table 3Table *1* Apparent activation energies of propane conversion over different catalysts tested in the PDH reaction in the temperature range of 500-550 °C., for fresh TiO_2 or it supported catalyst, the surface area significantly decreased from 119 to 53 m^2 g^{-1} after catalyst preparation and further decreased to 35 m^2 g^{-1} after about 60 h durability test. The surface areas of other catalysts also decreased but to a lower extent and are about 2-3.5 times higher than that of spent ZnO//TiO_2 after 8 PDH/regeneration cycles (Table 3). Therefore, we put forward that the loss of surface of TiO_2 could be another reason for catalyst deactivation due to a decrease in the number of active surface sites. A similar phenomenon was observed in our previous study dealing with Zr-

modified ZnO/TiO_2 catalysts[36]. When Zr was introduced to ZnO/TiO_2 catalyst, the sintering of TiO_2 was suppressed to some extent. The temperature-induced shrinkage of TiO_2 also affects the concentration of OH groups, which are required to in situ form ZnO_x species. As proven by *in-situ* DRIFTS, the intensity of defective OH groups (3200-3500 cm^{-1}) on the surface of bare TiO_2 support decreased strongly at 550 °C within first 30 min in a mixture of 50 vol% H_2 in Ar (Figure S6).

Table 3 The constants of catalyst deactivation, and surface area (S_{BET}) of fresh, as-prepared and spent (after about 60 h durability test) samples.

name	$S_{BET,\ bare\ support}$ / $m^2\ g^{-1}$	$S_{BET,\ as\text{-}prepared}$/ $m^2\ g^{-1}$[a]	$S_{BET,\ spent}$ / $m^2\ g^{-1}$[b]	$k_{deactivation}$ /h^{-1}
$ZnO\text{-}TiO_2$	119	53	35	0.66
$ZnO\text{-}LaZrO_x$	74	70	65	2.63
$ZnO\text{-}SiZrO_x$	166	156	125	0.78
$ZnO\text{-}TiZrO_x$	195	180	100	1.41

a obtained over the catalysts synthesized in 50 vol% H_2 in N_2 for 2 h.
b the catalysts were collected after 8 PDH/regeneration cycles.

The average propane selectivity values within one PDH cycle over the $ZnO//TiZrO_x$, $ZnO//TiO_2$, $ZnO//SiZrO_x$ and $ZnO//LaZrO_x$ are 95.6%, 93.0%, 93.1% and 88.5%, respectively (Figure S5). It should be specially mentioned that the catalysts showed similar degrees of initial propane conversion (Figure S4). The $ZnO//TiZrO_x$ is the most selective catalyst due to its lower ability to catalyze consecutive propene reactions leading to cracking products and coke (Figure S5). The corresponding averaged selectivity values are about 1% and 4%, respectively.

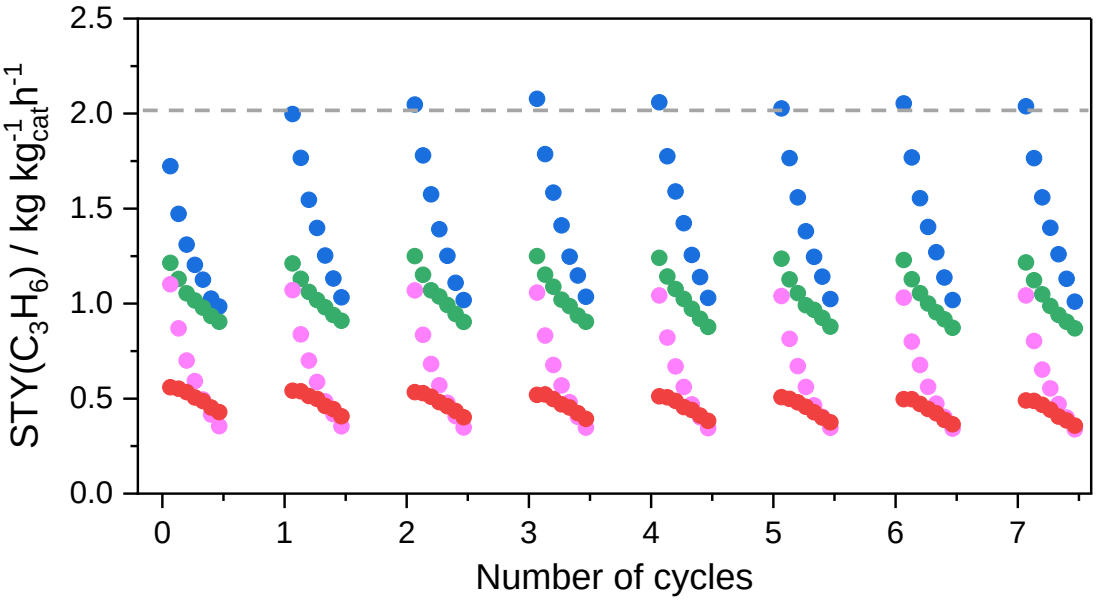

Figure 4 On-stream profiles of space-time yield (STY) of propene formation over different catalysts in a series of 8 PDH cycles. The catalysts were oxidatively regenerated after each cycle. The catalysts were loaded into reactors as shown in Figure 1(a). PDH conditions: 550 °C, 50 mg of support, 20 mg of commercial ZnO, C_3H_8/N_2=4:6, WHSV(C_3H_8) is 9.43, 5.66, 5.66, 2.83 and 2.83 h^{-1} for ZnO//$TiZrO_x$(●), ZnO//$SiZrO_x$(●), ZnO//$LaZrO_x$(●) and ZnO//TiO_2(●), respectively. Prior to the reaction, the catalysts were reduced in 50 vol% H_2 in N_2 at 550 °C for 2 h. After the 28 min PDH test, the catalysts were exposed to an air flow (10 mL min^{-1}) to remove coke. Afterwards, an additional reduction process (10 mL min^{-1}, 50 vol%H_2, 30 min) was carried out. The dashed line was added for guiding the eye.

We also compared the developed catalysts in terms of space time yield (STY) of propene formation. Except for the first cycle, the STY of ZnO//$TiZrO_x$ is about 2.0 kg kg^{-1}_{cat} h^{-1} and is comparable with that of ZnO-S-1_3[27], which is up to now one of the most active ZnO-based catalysts. The lower STY in the first cycle can be due to the smaller amount of Zn loading after the first 2 h reduction. The ZnO loading may increase further with rising reduction time and positively affects the rate of propene formation ZnO//$TiZrO_x$ (Table 1). Nevertheless, no significant decrease in STY after the second PDH cycle could be established (Figure 4). This is

also valid for ZnO//$SiZrO_x$ and ZnO//$LaZrO_x$, which showed lower STY values of 1.2 and 1.1 kg_{C3H6} kg^{-1}_{cat} h^{-1}, respectively. The least active and durable catalyst is ZnO//TiO_2.

For benchmarking purposes, we collected data for best-performing ZnO-based catalysts previously tested in the PDH reaction and compared them with the best material from the present study in terms of STY (Figure 5 and Table S1). To fairly compare the different catalysts, we used the ratio of experimentally determined propane conversion to the corresponding equilibrium propane conversion ($X(C_3H_8)/X(C_3H_8)eq$), because the latter strongly depends on the reaction temperature and the feed composition. Most of reported catalysts were tested at $X(C_3H_8)/X(C_3H_8)eq$ of 0.4-0.9 (Figure 5). The data points in the light-yellow area in Figure 5 were obtained over the catalysts developed in the current study and tested at about 50% of equilibrium conversion at 550 °C. The ZnO//$TiZrO_x$ catalyst with STY of 1.99 kg kg^{-1}_{cat} h^{-1} outperform many state-of-the-art catalysts tested at the same or even higher temperatures. Even the less active ZnO//TiO_2 catalyst in the present study outperformed two ZnO-based catalysts in the literature at a similar degree of propane conversion [19, 37].

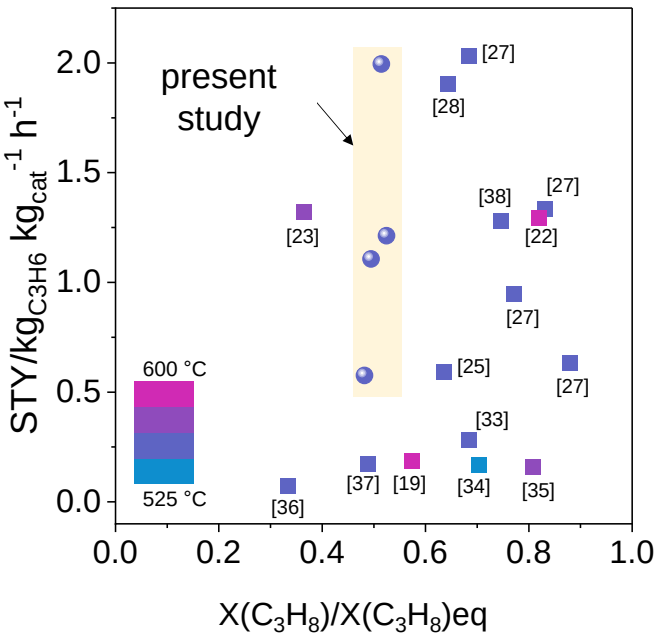

Figure 5 A comparison of ZnO//support catalysts developed in the present study with the state-of-the-art ZnO_x-based catalysts in terms of STY[19, 22, 23, 25, 27, 28, 35-40]. The data are available in Table S1.

4 Conclusions

We have demonstrated that catalysts simply consisting of a layer of ZnO on top of a layer of commercially available supports based on oxides of zirconium or titanium show high activity and durability in the PDH reaction. ZnO_x species on the surface of the supports are formed in situ under reaction conditions. Ex situ XAS analysis excluded the presence of ZnO (sub)nanoclusters but identified exclusively isolated ZnO_x species which geometry depends on the kind of metal oxide support. H_2 formation was identified as the rate-determining step in the course of PDH reaction. The presence of Ti in the support seems to facilitate this step. This knowledge sheds light on the reaction mechanisms and together with the simplicity of the catalyst preparation method opens the possibilities to purposefully develop PDH catalysts based on ZnO.

CRediT authorship contribution statement

Dan Zhao (DZ), Vita A. Kondratenko (VAK), Dmitry E. Doronkin (DED), Shanlei Han (SH): Investigation, Data curation, Formal analysis, Writing - original draft. **Jan-Dierk Grunwaldt (JDG), Uwe Rodemerck (UR), David Linke (DL):** Data curation, Formal analysis, Writing - review & editing. **Evgenii V. Kondratenko (EVK):** Conceptualization, Supervision, Writing - review & editing.

Declaration of Competing Interest

The authors declare no competing financial interest.

Data availability

The data can be provided upon reasonable requests.

Acknowledgements

Financial support by Deutsche Forschungsgemeinschaft (KO2261/8-1) and the State of Mecklenburg-Vorpommern is gratefully acknowledged. The authors also acknowledge DESY(Hamburg, Germany), a member of the Helmholtz Association HGF, for the provision of experimental facilities. Parts of this research were carried out at PETRA III, and the authors would like to thank Dr. Edmund Welter for assistance in using beamline P65. Beamtime was allocated for proposal I-20210242.

References

[1] T. Otroshchenko, G. Jiang, V.A. Kondratenko, U. Rodemerck, E.V. Kondratenko, Current status and perspectives in oxidative, non-oxidative and CO_2-mediated dehydrogenation of propane and isobutane over metal oxide catalysts, Chem Soc Rev, 50 (2021) 473-527.

[2] C. Li, G. Wang, Dehydrogenation of light alkanes to mono-olefins, Chem Soc Rev, 50 (2021) 4359-4381.

[3] S. Chen, X. Chang, G. Sun, T. Zhang, Y. Xu, Y. Wang, C. Pei, J. Gong, Propane dehydrogenation: catalyst development, new chemistry, and emerging technologies, Chem Soc Rev, 50 (2021) 3315-3354.

[4] G. Liu, Z.-J. Zhao, T. Wu, L. Zeng, J. Gong, Nature of the Active Sites of VO_x/Al_2O_3 Catalysts for Propane Dehydrogenation, ACS Catalysis, 6 (2016) 5207-5214.

[5] U. Rodemerck, M. Stoyanova, E.V. Kondratenko, D. Linke, Influence of the kind of VO_x structures in VO_x/MCM-41 on activity, selectivity and stability in dehydrogenation of propane and isobutane, Journal of Catalysis, 352 (2017) 256-263.

[6] Z.J. Zhao, T. Wu, C. Xiong, G. Sun, R. Mu, L. Zeng, J. Gong, Hydroxyl-Mediated Non-oxidative Propane Dehydrogenation over VO_x/gamma-Al_2O_3 Catalysts with Improved Stability, Angew Chem Int Ed Engl, 57 (2018) 6791-6795.

[7] J.J. Sattler, I.D. Gonzalez-Jimenez, L. Luo, B.A. Stears, A. Malek, D.G. Barton, B.A. Kilos, M.P. Kaminsky, T.W. Verhoeven, E.J. Koers, M. Baldus, B.M. Weckhuysen, Platinum-promoted Ga/Al_2O_3 as highly active, selective, and stable catalyst for the dehydrogenation of propane, Angew Chem Int Ed Engl, 53 (2014) 9251-9256.

[8] Y. Dai, J. Gu, S. Tian, Y. Wu, J. Chen, F. Li, Y. Du, L. Peng, W. Ding, Y. Yang, γ-Al_2O_3 sheet-stabilized isolate Co^{2+} for catalytic propane dehydrogenation, Journal of Catalysis, 381 (2020) 482-492.

[9] C. Chen, S. Zhang, Z. Wang, Z.-Y. Yuan, Ultrasmall Co confined in the silanols of dealuminated beta zeolite: A highly active and selective catalyst for direct dehydrogenation of propane to propylene, Journal of Catalysis, 383 (2020) 77-87.

[10] B. Hu, N.M. Schweitzer, G. Zhang, S.J. Kraft, D.J. Childers, M.P. Lanci, J.T. Miller, A.S. Hock, Isolated Fe^{II} on Silica As a Selective Propane Dehydrogenation Catalyst, ACS Catalysis, 5 (2015) 3494-3503.

[11] G. Wang, H. Zhang, Q. Zhu, X. Zhu, X. Li, H. Wang, C. Li, H. Shan, Sn-containing hexagonal mesoporous silica (HMS) for catalytic dehydrogenation of propane: An efficient strategy to enhance stability, Journal of Catalysis, 351 (2017) 90-94.

[12] Z. Maeno, S. Yasumura, X. Wu, M. Huang, C. Liu, T. Toyao, K.I. Shimizu, Isolated Indium Hydrides in CHA Zeolites: Speciation and Catalysis for Nonoxidative Dehydrogenation of Ethane, J Am Chem Soc, 142 (2020) 4820-4832.

[13] T. Otroshchenko, S. Sokolov, M. Stoyanova, V.A. Kondratenko, U. Rodemerck, D. Linke, E.V. Kondratenko, ZrO_2-Based Alternatives to Conventional Propane Dehydrogenation Catalysts: Active Sites, Design, and Performance, Angew Chem Int Ed Engl, 54 (2015) 15880-15883.

[14] Y. Zhang, Y. Zhao, T. Otroshchenko, H. Lund, M.M. Pohl, U. Rodemerck, D. Linke, H. Jiao, G. Jiang, E.V. Kondratenko, Control of coordinatively unsaturated Zr sites in ZrO_2 for efficient C-H bond activation, Nat Commun, 9 (2018) 3794.

[15] C.-F. Li, X. Guo, Q.-H. Shang, X. Yan, C. Ren, W.-Z. Lang, Y.-J. Guo, Defective TiO_2 for Propane Dehydrogenation, Industrial & Engineering Chemistry Research, 59 (2020) 4377-4387.

[16] Z. Xie, T. Yu, W. Song, J. Li, Z. Zhao, B. Liu, Z. Gao, D. Li, Highly Active Nanosized Anatase TiO_{2-x} Oxide Catalysts In Situ Formed through Reduction and Ostwald Ripening Processes for Propane Dehydrogenation, ACS Catalysis, 10 (2020) 14678-14693.

[17] D. Zhao, H. Lund, U. Rodemerck, D. Linke, G. Jiang, E.V. Kondratenko, Revealing fundamentals affecting activity and product selectivity in non-oxidative propane dehydrogenation over bare Al_2O_3, Catalysis Science & Technology, 11 (2021) 1386-1394.

[18] P. Wang, Z. Xu, T. Wang, Y. Yue, X. Bao, H. Zhu, Unmodified bulk alumina as an efficient catalyst for propane dehydrogenation, Catalysis Science & Technology, 10 (2020) 3537-3541.

[19] C. Chen, Z. Hu, J. Ren, S. Zhang, Z. Wang, Z.-Y. Yuan, ZnO Nanoclusters Supported on Dealuminated Zeolite β as a Novel Catalyst for Direct Dehydrogenation of Propane to Propylene, ChemCatChem, 11 (2019) 868-877.

[20] C. Chen, Z.-P. Hu, J.-T. Ren, S. Zhang, Z. Wang, Z.-Y. Yuan, ZnO supported on high-silica HZSM-5 as efficient catalysts for direct dehydrogenation of propane to propylene, Molecular Catalysis, 476 (2019).

[21] J. Liu, Y. Liu, H. Liu, Y. Fu, Z. Chen, W. Zhu, Silicalite-1 Supported ZnO as an Efficient Catalyst for Direct Propane Dehydrogenation, ChemCatChem, 13 (2021) 4780-4786.

[22] S. Song, K. Yang, P. Zhang, Z. Wu, J. Li, H. Su, S. Dai, C. Xu, Z. Li, J. Liu, W. Song, Silicalite-1 Stabilizes Zn-Hydride Species for Efficient Propane Dehydrogenation, ACS Catalysis, (2022) 5997-6006.

[23] L. Xie, R. Wang, Y. Chai, X. Weng, N. Guan, L. Li, Propane dehydrogenation catalyzed by in-situ partially reduced zinc cations confined in zeolites, Journal of Energy Chemistry, 63 (2021) 262-269.

[24] B. Wan, H.M. Chu, Reaction kinetics of propane dehydrogenation over partially reduced zinc oxide supported on silicalite, J. Chem. SoC. Faraday. Trans., 88 (1992) 2943-2947.

[25] D. Zhao, K. Guo, S. Han, D.E. Doronkin, H. Lund, J. Li, J.-D. Grunwaldt, Z. Zhao, C. Xu, G. Jiang, E.V. Kondratenko, Controlling Reaction-Induced Loss of Active Sites in ZnO_x/Silicalite-1 for Durable Nonoxidative Propane Dehydrogenation, ACS Catalysis, 12 (2022) 4608-4617.

[26] D. Zhao, Y. Li, S. Han, Y. Zhang, G. Jiang, Y. Wang, K. Guo, Z. Zhao, C. Xu, R. Li, C. Yu, J. Zhang, B. Ge, E.V. Kondratenko, ZnO Nanoparticles Encapsulated in Nitrogen-Doped Carbon Material and Silicalite-1 Composites for Efficient Propane Dehydrogenation, iScience, 13 (2019) 269-276.

[27] D. Zhao, X. Tian, D.E. Doronkin, S. Han, V.A. Kondratenko, J.D. Grunwaldt, A. Perechodjuk, T.H. Vuong, J. Rabeah, R. Eckelt, U. Rodemerck, D. Linke, G. Jiang, H. Jiao, E.V. Kondratenko, In situ formation of ZnO_x species for efficient propane dehydrogenation, Nature, 599 (2021) 234-238.

[28] D. Zhao, M. Gao, X. Tian, D.E. Doronkin, S. Han, J.-D. Grunwaldt, U. Rodemerck, D. Linke, M. Ye, G. Jiang, H. Jiao, E.V. Kondratenko, Effect of Diffusion Constraints and ZnO_x Speciation on

Nonoxidative Dehydrogenation of Propane and Isobutane over ZnO-Containing Catalysts, ACS Catalysis, 13 (2023) 3356-3369.

[29] H.Y. Zhang, B. Xie, X.J. Meng, U. Muller, B. Yilmaz, M. Feyen, S. Maurer, H. Gies, T. Tatsumi, X.H. Bao, W.P. Zhang, D. De Vos, F.S. Xiao, Rational synthesis of Beta zeolite with improved quality by decreasing crystallization temperature in organotemplate-free route, Micropor Mesopor Mat, 180 (2013) 123-129.

[30] B. Ravel, M. Newville, ATHENA, ARTEMIS, HEPHAESTUS: data analysis for X-ray absorption spectroscopy using IFEFFIT, J Synchrotron Radiat, 12 (2005) 537-541.

[31] J. Perezramirez, E. Kondratenko, Evolution, achievements, and perspectives of the TAP technique, Catalysis Today, 121 (2007) 160-169.

[32] K. Morgan, N. Maguire, R. Fushimi, J.T. Gleaves, A. Goguet, M.P. Harold, E.V. Kondratenko, U. Menon, Y. Schuurman, G.S. Yablonsky, Forty years of temporal analysis of products, Catalysis Science & Technology, 7 (2017) 2416-2439.

[33] J.T. Gleaves, G.S. Yablonskii, P. Phanawadee, Y. Schuurman, TAP-2: An interrogative kinetics approach, Applied Catalysis A: General 160 (1997) 55-88.

[34] M. Soick, D. Wolf, M. Baerns, Determination of kinetic parameters for complex heterogeneous catalytic reactions by numerical evalution of TAP experiments, Chemical Engineering Science, 55 (2000) 2875-2882.

[35] S. Han, D. Zhao, T. Otroshchenko, H. Lund, U. Bentrup, V.A. Kondratenko, N. Rockstroh, S. Bartling, D.E. Doronkin, J.-D. Grunwaldt, U. Rodemerck, D. Linke, M. Gao, G. Jiang, E.V. Kondratenko, Elucidating the Nature of Active Sites and Fundamentals for their Creation in Zn-Containing ZrO_2–Based Catalysts for Nonoxidative Propane Dehydrogenation, ACS Catalysis, 10 (2020) 8933-8949.

[36] S. Han, D. Zhao, H. Lund, N. Rockstroh, S. Bartling, D.E. Doronkin, J.-D. Grunwaldt, M. Gao, G. Jiang, E.V. Kondratenko, TiO_2-Supported catalysts with ZnO and ZrO_2 for non-oxidative dehydrogenation of propane: mechanistic analysis and application potential, Catalysis Science & Technology, 10 (2020) 7046-7055.

[37] C. Chen, M. Sun, Z. Hu, J. Ren, S. Zhang, Z.-Y. Yuan, New insight into the enhanced catalytic performance of ZnPt/HZSM-5 catalysts for direct dehydrogenation of propane to propylene, Catalysis Science & Technology, 9 (2019) 1979-1988.

[38] Y.-n. Sun, C. Gao, L. Tao, G. Wang, D. Han, C. Li, H. Shan, Zn Nb O catalysts for propylene production via catalytic dehydrogenation of propane, Catalysis Communications, 50 (2014) 73-77.

[39] X. Shi, S. Chen, S. Li, Y. Yang, Q. Guan, J. Ding, X. Liu, Q. Liu, W. Xu, J. Lu, Particle size effect of SiO_2-supported ZnO catalysts in propane dehydrogenation, Catalysis Science & Technology, 13 (2023) 1866-1873.

[40] F. Yang, J. Zhang, Z. Shi, J. Chen, G. Wang, J. Zhao, R. Zhuo, R. Wang, Regulation of Active ZnO Species on Si-based Supports with Diverse Textural Properties for Efficient Propane Dehydrogenation, ChemCatChem, 15 (2023), No. e2023004.

Graphical abstract

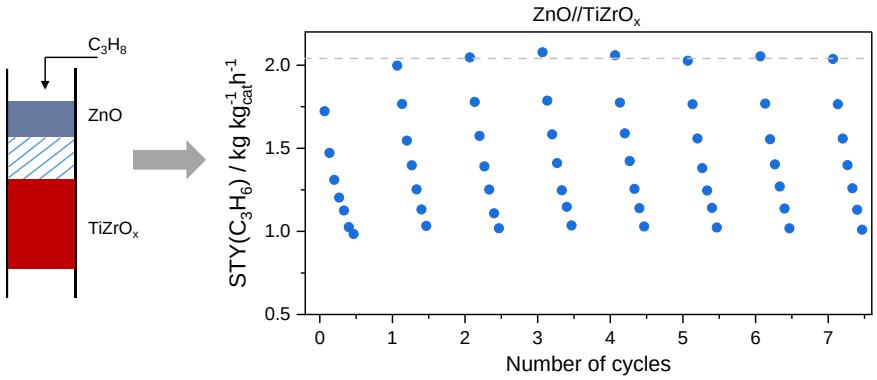

Supporting Information for

Effect of supports on the kind of in-situ formed ZnO_x species and its consequence for non-oxidative propane dehydrogenation

Dan Zhao[a, §], Vita A. Kondratenko[a], Dmitry E. Doronkin[b], Shanlei Han[a], Jan-Dierk Grunwaldt[b], Uwe Rodemerck[a], David Linke[a], Evgenii V. Kondratenko[a*]

[a] Leibniz-Institut für Katalyse e. V., 18059 Rostock, Germany

[b]Institute of Catalysis Research and Technology and Institute for Chemical Technology and Polymer Chemistry, Karlsruhe Institute of Technology (KIT), 76131 Karlsruhe, Germany

[§]Current address: Institute of Catalysis Research and Technology, Karlsruhe Institute of Technology (KIT), 76344 Eggenstein-Leopoldshafen, Germany

*Correspondence to evgenii.kondratenko@catalysis.de

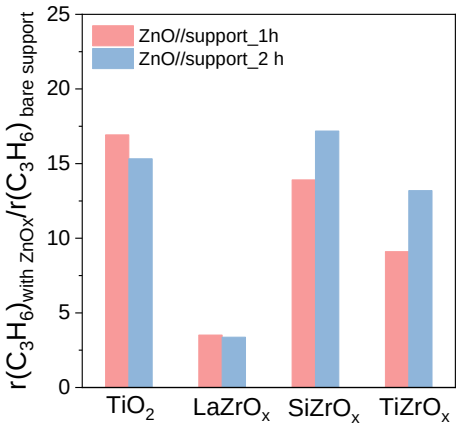

Figure S1 The ratio of the rate of propene formation over ZnO_x-containing catalysts to that of bare supports.

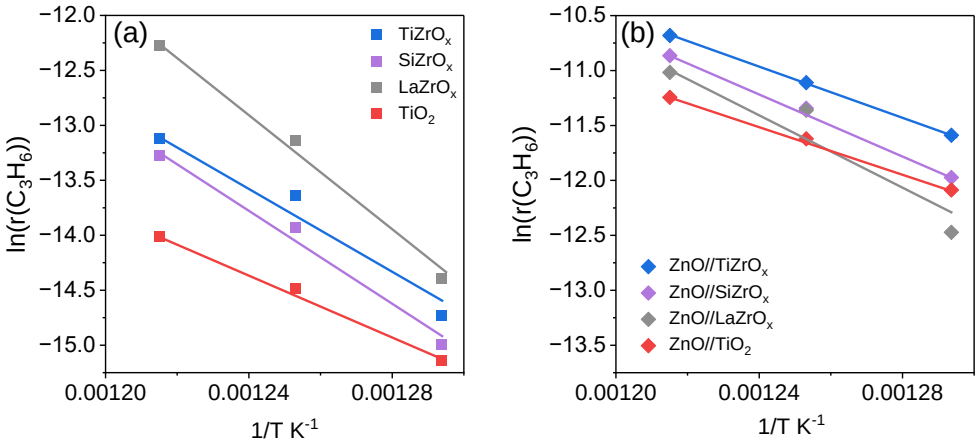

Figure S2 The Arrhenius plots of propene formation rate over (a) bare supports and (b) ZnO-containing samples tested using a fed of C_3H_8:N_2 = 2:3 at 550 °C. The conversion of propane was controlled below 15% of the equilibrium conversion, which is about 42% at 550 °C using a feed of C_3H_8:N_2 = 2:3.

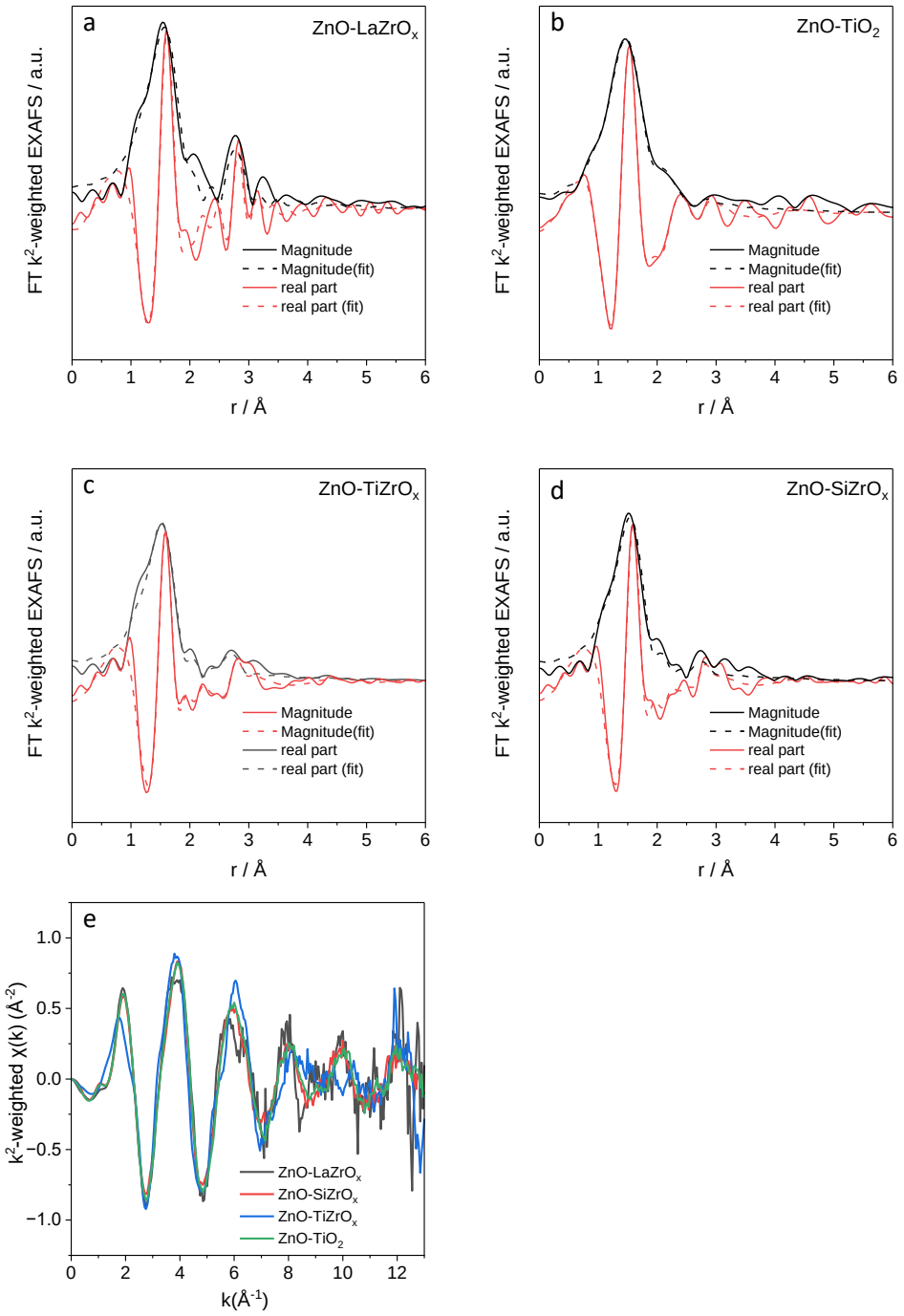

Figure S3 k^2-weighted EXAFS functions (extracted fine structure in k-space) of as-prepared catalysts and reference materials; the EXAFS fits for (a) ZnO-LaZrO$_x$, (b) ZnO-TiO$_2$, (c) ZnO-TiZrO$_x$ and (d) ZnO-SiZrO$_x$ in r space; the k^2-weighted χ(k) in k-space; (e) the raw data of EXAFS over different samples.

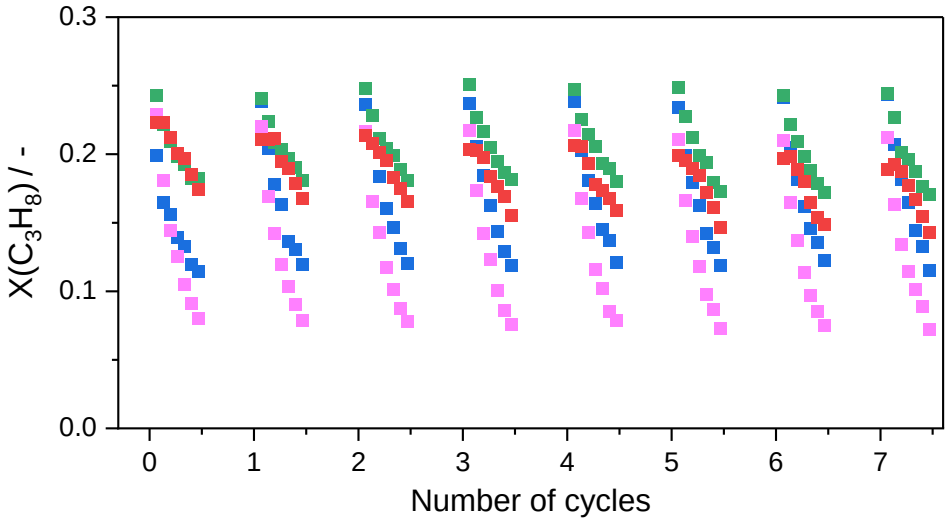

Figure S4 Propane conversion over ZnO//$TiZrO_x$(■), ZnO/$ZrSiO_x$(■), ZnO//$LaZrO_x$(■) and ZnO//TiO_2(■) catalyst. All the catalysts were loaded as shown in Figure 1(a). Reaction conditions: 550 °C, 50 mg of support, 20 mg of C-ZnO, C_3H_8:N_2=4:6, WHSV(C_3H_8) is 9.43, 5.66, 5.66, 2.83 and 2.83 h^{-1} for ZnO//$TiZrO_x$, ZnO//$ZrSiO_x$, ZnO//$LaZrO_x$ and ZnO//TiO_2, respectively. Prior to the test, the catalysts were reduced in 50 vol% H_2 in N_2 at 550 °C for 2 h. After 28 min PDH tests, the catalysts were exposed to an air flow (10 mL min^{-1}) to remove coke. Afterwards, an additional reduction process (10 mL min^{-1}, 50 vol%H_2, 30 min) was carried out.

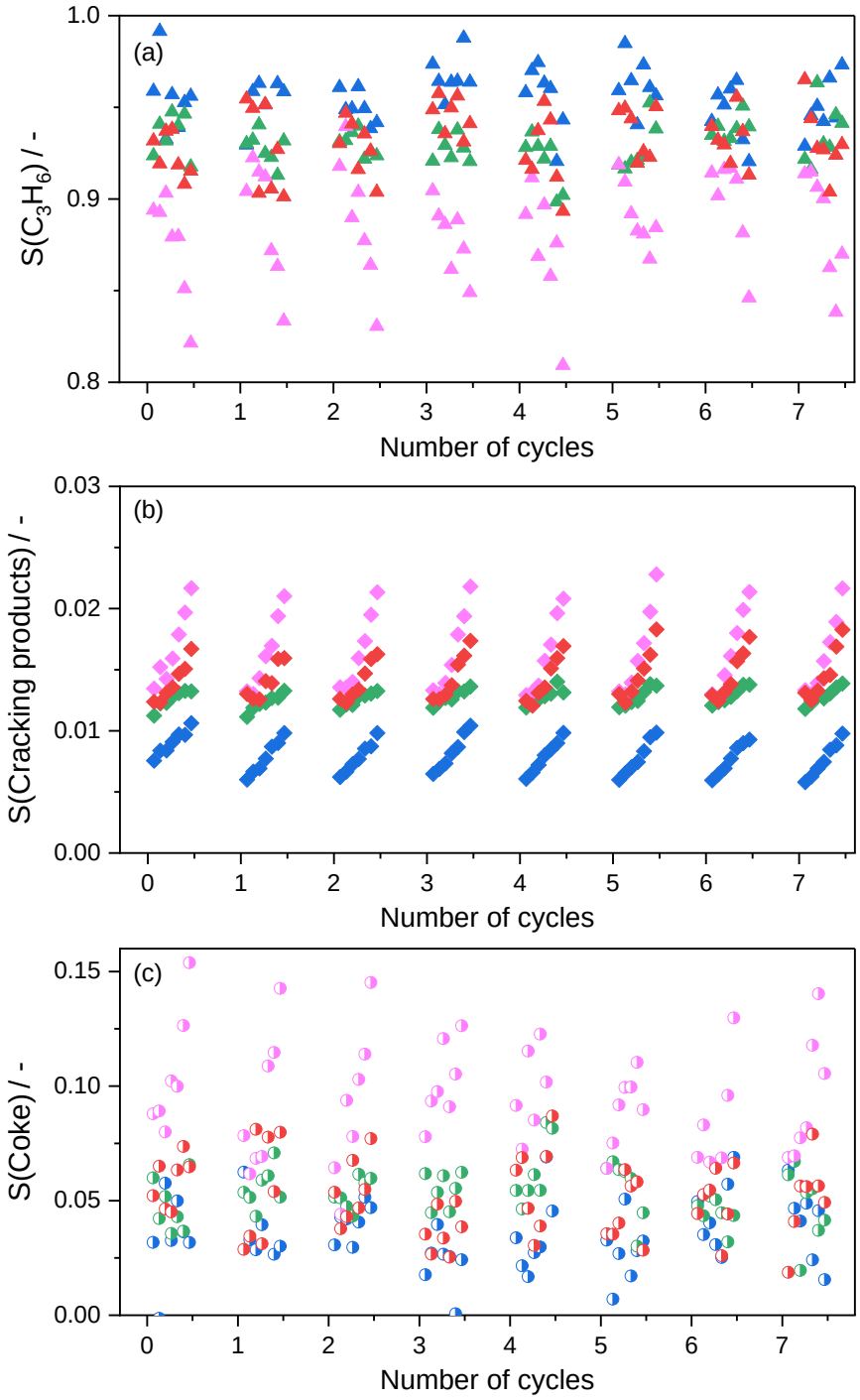

Figure S5 The selectivity to propene (a), to cracking products (b) and to coke (c) over ZnO//$TiZrO_x$(▲♦◐), ZnO/$ZrSiO_x$(▲◆◐), ZnO//$LaZrO_x$(▲◆◐) and ZnO//TiO_2(▲◆◐) catalyst. All the catalysts were loaded as shown in Figure 1(a). Reaction conditions: 550 °C, 50 mg of support, 20 mg of C-ZnO, C_3H_8:N_2=4:6, WHSV(C_3H_8) is 9.43, 5.66, 5.66, 2.83 and 2.83 h^{-1} for ZnO//$TiZrO_x$, ZnO//$ZrSiO_x$, ZnO//$LaZrO_x$ and ZnO//TiO_2, respectively. Prior to the test, the catalysts were reduced in 50 vol% H_2 in N_2 at 550 °C for 2 h. After 28 min PDH tests, the catalysts were exposed to an air flow (10 mL min^{-1}) to remove coke. Afterwards, an additional reduction process (10 mL min^{-1}, 50 vol%H_2, 30 min) was carried out.

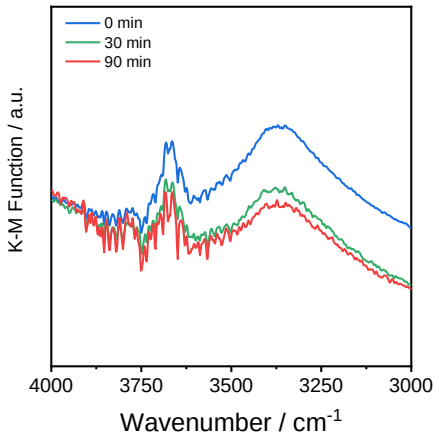

Figure S6 In-situ DRIFTS recorded over TiO_2 in a flow of 50 vol% H_2 in Ar at 550 °C

Table S1 A comparison of the developed ZnO_x-catalysts and the-state-of-the-art catalysts in terms of space time yield of C_3H_6

Catalysts	T /°C	feed	$X(C_3H_8)$	$X(C_3H_8)_{eq}$	$X(C_3H_8)/X(C_3H_8)_{eq}$	$STY(C_3H_6)$	Ref.
10%ZnO/deAl beta	600	C_3H_8:N_2 =5:95	0.533	0.93	0.57	0.19	[1]
10%ZnO0.1Pt/HZSM-5	525	C_3H_8:N_2 =5:95	0.520	0.74	0.70	0.17	[2]
6%ZnO/S-1	550	C_3H_8:N_2 =4:6	0.295	0.46	0.64	0.59	[3]
Zn-4@S-1	580	C_3H_8:N_2 =1:9	0.30	0.82	0.36	1.32	[4]
4ZnO/$TiZrO_x$	550	C_3H_8:N_2:H_2 =40:55:5	0.30	0.40	0.75	1.28	[5]
2Zn1.4Zr/TiO_2	550	C_3H_8:N_2:H_2 =4:4:2	0.20	0.29	0.68	0.28	[6]
Zn-H/Silicalite-1	600	C_3H_8:N_2:H_2 =4:4:2	0.43	0.53	0.82	1.29	[7]
Zn-Nb-O	580	~100%C_3H_8	0.33	0.42	0.81	0.16	[8]
ZnO-S-1_3	550	C_3H_8:N_2 =4:6	0.31	0.46	0.67	2.04	[9]
ZnO-S-1_3	550	C_3H_8:N_2:H_2 =4:4:2	0.26	0.29	0.88	0.63	[9]
ZnO-S-1_3	550	C_3H_8:N_2 =7:3	0.31	0.38	0.83	1.33	[9]
ZnO-S-1_3	550	C_3H_8:N_2 =4:6	0.36	0.46	0.77	0.95	[9]
ZnO-deAl-Beta	550	C_3H_8:N_2 =4:6	0.30	0.46	0.64	1.90	[10]
ZnO//$TiZrO_x$	550	C_3H_8:N_2 =4:6	0.24	0.46	0.51	1.99	This work
ZnO//TiO_2	550	C_3H_8:N_2 =4:6	0.22	0.46	0.48	0.58	This work
ZnO//$ZrSiO_2$	550	C_3H_8:N_2 =4:6	0.24	0.46	0.52	1.21	This work
ZnO//$LaZrO_x$	550	C_3H_8:N_2 =4:6	0.23	0.46	0.49	1.11	This work

References:

[1] C. Chen, Z. Hu, J. Ren, S. Zhang, Z. Wang, Z.-Y. Yuan, ZnO Nanoclusters Supported on Dealuminated Zeolite β as a Novel Catalyst for Direct Dehydrogenation of Propane to Propylene, ChemCatChem, 11 (2019) 868-877.

[2] C. Chen, M. Sun, Z. Hu, J. Ren, S. Zhang, Z.-Y. Yuan, New insight into the enhanced catalytic performance of ZnPt/HZSM-5 catalysts for direct dehydrogenation of propane to propylene, Catalysis Science & Technology, 9 (2019) 1979-1988.

[3] D. Zhao, K. Guo, S. Han, D.E. Doronkin, H. Lund, J. Li, J.-D. Grunwaldt, Z. Zhao, C. Xu, G. Jiang, E.V. Kondratenko, Controlling Reaction-Induced Loss of Active Sites in ZnO_x/Silicalite-1 for Durable Nonoxidative Propane Dehydrogenation, ACS Catalysis, 12 (2022) 4608-4617.

[4] L. Xie, R. Wang, Y. Chai, X. Weng, N. Guan, L. Li, Propane dehydrogenation catalyzed by in-situ partially reduced zinc cations confined in zeolites, Journal of Energy Chemistry, 63 (2021) 262-269.

[5] S. Han, D. Zhao, T. Otroshchenko, H. Lund, U. Bentrup, V.A. Kondratenko, N. Rockstroh, S. Bartling, D.E. Doronkin, J.-D. Grunwaldt, U. Rodemerck, D. Linke, M. Gao, G. Jiang, E.V. Kondratenko, Elucidating the Nature of Active Sites and Fundamentals for their Creation in Zn-Containing ZrO_2–Based Catalysts for Nonoxidative Propane Dehydrogenation, ACS Catalysis, 10 (2020) 8933-8949.

[6] S. Han, D. Zhao, H. Lund, N. Rockstroh, S. Bartling, D.E. Doronkin, J.-D. Grunwaldt, M. Gao, G. Jiang, E.V. Kondratenko, TiO_2-Supported catalysts with ZnO and ZrO_2 for non-oxidative dehydrogenation of propane: mechanistic analysis and application potential, Catalysis Science & Technology, 10 (2020) 7046-7055.

[7] S. Song, K. Yang, P. Zhang, Z. Wu, J. Li, H. Su, S. Dai, C. Xu, Z. Li, J. Liu, W. Song, Silicalite-1 Stabilizes Zn-Hydride Species for Efficient Propane Dehydrogenation, ACS Catalysis, (2022) 5997-6006.

[8] Y.-n. Sun, C. Gao, L. Tao, G. Wang, D. Han, C. Li, H. Shan, Zn Nb O catalysts for propylene production via catalytic dehydrogenation of propane, Catalysis Communications, 50 (2014) 73-77.

[9] D. Zhao, X. Tian, D.E. Doronkin, S. Han, V.A. Kondratenko, J.D. Grunwaldt, A. Perechodjuk, T.H. Vuong, J. Rabeah, R. Eckelt, U. Rodemerck, D. Linke, G. Jiang, H. Jiao, E.V. Kondratenko, In situ formation of ZnO_x species for efficient propane dehydrogenation, Nature, 599 (2021) 234-238.

[10] D. Zhao, M. Gao, X. Tian, D.E. Doronkin, S. Han, J.-D. Grunwaldt, U. Rodemerck, D. Linke, M. Ye, G. Jiang, H. Jiao, E.V. Kondratenko, Effect of Diffusion Constraints and ZnO_x Speciation on Nonoxidative Dehydrogenation of Propane and Isobutane over ZnO-Containing Catalysts, ACS Catalysis, 13 (2023) 3356-3369.